Molecular Crystals and Liquid Crystals

ISSN: 1542-1406 (Print) 1563-5287 (Online) Journal homepage: http://www.tandfonline.com/loi/gmcl20

Influence Sputtering Conditions on Electrical Characteristics of Si-$LiNbO_3$ Heterostructures Formed by Radio-Frequency Magnetron Sputtering

M. Sumets, V. Ievlev, A. Kostyuchenko & V. Kuz'mina

To cite this article: M. Sumets, V. Ievlev, A. Kostyuchenko & V. Kuz'mina (2014) Influence Sputtering Conditions on Electrical Characteristics of Si-$LiNbO_3$ Heterostructures Formed by Radio-Frequency Magnetron Sputtering, Molecular Crystals and Liquid Crystals, 603:1, 202-215, DOI: 10.1080/15421406.2014.967607

To link to this article: http://dx.doi.org/10.1080/15421406.2014.967607

Published online: 15 Dec 2014.

Mol. Cryst. Liq. Cryst., Vol. 603: pp. 202–215, 2014

ISSN: 1542-1406 print/1563-5287 online
DOI: 10.1080/15421406.2014.967607

Influence Sputtering Conditions on Electrical Characteristics of Si-$LiNbO_3$ Heterostructures Formed by Radio-Frequency Magnetron Sputtering

M. SUMETS,[1,2,*] V. IEVLEV,[1] A. KOSTYUCHENKO,[1] AND V. KUZ'MINA[1]

[1]Voronezh State University, Universitetskaya Square, 1 394000, Voronezh, Russia
[2]Voronezh Institute of the State Fire Service of Russian Emergencies Ministry, Krasnoznamennaya st. 231, 394052, Voronezh, Russia

Polycrystalline $LiNbO_3$ films on (001)Si substrate were grown by radio-frequency magnetron sputtering process at different sputtering conditions. X-ray diffraction analysis showed that films formed in Ar environment ($P = 5.0 \times 10^{-1}$ Pa) having two-phase composition ($LiNbO_3$, $LiNb_3O_8$) transformed into c-axes-oriented $LiNbO_3$ films when Ar pressure declined up to $P = 1.5 \times 10^{-1}$ Pa. This induced an increase in positive oxide charge and coercive field due to formation of defects in the $LiNbO_3$ layer. Using $Ar + O_2$ reactive gas mixture led to decline in defect formation (positive oxide charge) and coercive field. Current-voltage and capacitance-voltage analyses demonstrated that barrier properties of the Si-$LiNbO_3$ heterojunctions are affected by the plasma composition.

Keywords Lithium niobate; thin films; heterojunctions; ferroelectrics; electrical properties; sputtering

1. Introduction

Lithium niobate is an attractive material for integrated electronics due to its unique electro-optical and opto-acoustic properties. Various techniques are applied for creating thin $LiNbO_3$ films on different substrates: sol-gel method [1], pulsed laser deposition [2], liquid-phase epitaxy [3], and chemical vapor deposition from vapor phase (CVD process) [4]. Radio-frequency (RF) magnetron sputtering (RFMS) being an effective vacuum method allows preservation of the initial elemental composition of grown complex oxides [5–7]. Depending on the purpose, a wide range of substrates are used such as sapphire, silicon, SiO_2, GaN, etc. Despite the lack of crystalline match of substrate with $LiNbO_3$ layers, capability of formation of thin $LiNbO_3$ films on silicon remains a big challenge because of miniaturization and hybridization with silicon technologies. It has been demonstrated [8–10] that technological conditions greatly influence the electrical and structural properties of Si-$LiNbO_3$ heterostructures. It is important to emphasize that electrical characteristics such as capacitance, ac and dc conductivity, and ferroelectric properties are affected by

*Address correspondence to M. Sumets, Voronezh Institute of the State Fire Service of Russian Emergencies Ministry, Krasnoznamennaya st., 231, 394052, Voronezh, Russia. Tel.: +7473 2424739; E-mail: maxsumets@gmail.com

bulk properties of $LiNbO_3$ as well as barrier conditions at the Si-$LiNbO_3$ interface [11, 12] and separation of these types of influence is an important issue.

In general, barrier conditions at the heterointerface depend on many factors: electron affinities of contacting materials, interface states, built-in charge, etc. It is generally accepted that when heterojunction film substrate is formed, the substrate temperature plays an important role because it is a driving force of reconstruction and relaxation which leads to decreased stress and mismatch at the interface and as a result interface state density declines [13, 14]. Regarding RFMS method, reactive gas composition is a crucial point because formation of complex oxides is very sensitive to the plasma properties. Many authors proposed [15–17] use of $Ar+O_2$ gas mixture as an appropriate reactive gas environment for RFMS process for formation of Si-LiNbO3 heterostructures with quite low interface state density. Nevertheless, despite the influence of this environment on ferroelectric properties, current-voltage (I–V) and capacitance-voltage (C–V) characteristics have been revealed in general, whereas detailed analysis of the interface conditions has not been carried out yet.

When two materials are brought in contact they exchange by electrons which leads to the formation of potential barriers at the interface as well as band offsets because of change in conduction and valence band edge energy. The magnitudes of changes in the band-edge energies are critically important for many devices such as random-access memory units, ferroelectric capacitors, etc. Taking into account that C-V and I-V characteristics of the heterostructures being powerful investigative tools, are greatly influenced by barrier properties [18, 19], it is important to study the electron phenomena at the Si-$LiNbO_3$ heterostructures formed in different technological conditions inside out.

Despite the various models describing the electrical properties of heterostructures, there are only few mechanisms related to the carrier transport through the potential barriers at the heterojunction. One of the most common phenomena is the Richardson-Schottky emission [20]. In this case, when voltage V is applied electrons overcome Shottky barrier formed between metal (or highly doped semiconductor) and semiconductor. In the framework of this emission current-voltage characteristics can be expressed by the following formula:

$$J = \frac{4\pi qm}{h^3}(kT)^2 \exp\left(-\frac{q\varphi}{kT}\right)\exp\left(\frac{\beta\sqrt{E}}{kT}\right) \tag{1}$$

where T is the temperature, k and h are Boltzmann's constant and Plank's constant, respectively, and q and m are the electron charge and mass, respectively, E is the electric field, and ϕ is the barrier height. β is a parameter that can be given as:

$$\beta = \frac{1}{2}\sqrt{\frac{q^3}{\pi\varepsilon\varepsilon_0}} \tag{2}$$

where ε and ε_0 are the dielectric constants of the layer and electric constant, respectively.

On the other hand, in solids, the following formula related to the Richardson-Schottky emission has been proposed by Simmons [20]:

$$J_{R-S} = 2q\left(\frac{2\pi m^* kT}{h^2}\right)^{\frac{3}{2}}\mu E \exp\left(-\frac{q\varphi}{kT}\right)\exp\left(\frac{\beta\sqrt{E}}{kT}\right) \tag{3}$$

where m^* and μ are the effective mass and mobility of the carriers of charge, respectively.

Equations (1) and (3) differ only by the pre-exponential factor, and the mobility of the charges and applied field are critical factors determining which formula is acceptable

in a certain case. On the other hand, in ferroelectrics, polarization as well as space charge phenomena greatly influence the barrier properties [21, 22]. As a result, barrier height can be reduced and the apparent potential barrier can be written as:

$$\varphi_{ap} = \varphi_b - \sqrt{\frac{qP}{4\pi\,(\varepsilon\varepsilon_0)^2}} \tag{4}$$

Here ϕ_b is the true value of potential barrier and P is the ferroelectric polarization. Moreover, parameter β in (2) can be expressed as [22]:

$$\beta = \sqrt{\frac{q^3 N_{ef}}{8\pi\varepsilon\varepsilon_0 P}} \tag{5}$$

Here N_{ef} is the effective impurity concentration in the depletion region.

In the case of high electric fields tunneling becomes a common mechanism of electron transmission through the potential barrier. At low temperatures the Fowler-Nordheim tunneling is prevalent [23]:

$$J_{F-N} = AE^2 \exp\left(-\frac{B}{E}\right) \tag{6}$$

where A is the constant related to the electron distribution and other factors, E is the electric field strength, and B is the constant of the material, which can be defined according to the following formula:

$$B = \frac{8\pi\sqrt{2m^*}\phi^{3/2}}{3qh} \tag{7}$$

where m^* is the effective mass of the electrons, h is the Planck's constant, and φ is the average height of the potential barrier.

In the range of intermediate temperatures thermal-assisted tunneling dominates and I–V characteristics can be described by the following expression [24]:

$$J = Js\left(\exp\left(\frac{V}{Vo}\right) - 1\right) \tag{8}$$

Here

$$\begin{aligned} Js &= \tfrac{A\cdot T}{k}\sqrt{qV_{oo}\pi}\sqrt{\tfrac{q\varphi_b}{\cosh\left(\left(\frac{qV_{oo}}{kT}\right)^2\right)}}\exp\left(-\tfrac{q\varphi_b}{V_o}\right) \\ V_o &= V_{oo}\coth\left(\tfrac{qV_{oo}}{kT}\right) \end{aligned} \tag{9}$$

and

$$V_{oo} = \frac{h}{4\pi}\sqrt{\frac{Nd}{m^*\varepsilon\varepsilon_0}} \tag{10}$$

In (10) N_d is concentration of ionized donors in the dielectric layer.

Also, in the case of the abrupt nn-junctions space charge effects such as space charge limited currents play an important role [25] and in the simplest approach I-V characteristics

can be expressed as follows:

$$J = \frac{9}{8}\varepsilon\varepsilon_0\mu\theta\frac{V^2}{d^3} \tag{11}$$

Here θ is the ratio free charge to the trapped charges, μ is the mobility of the carries, and d is the thickness of the film.

Therefore, it is important to separate all electron phenomena related to the heterojunction from bulk ones. The purpose of the present work was to study how sputtering conditions influence electrical properties of the Si-$LiNbO_3$ heterostructures in order to create the most suitable ones for memory applications.

2. Experimental

As has been investigated [26] gas pressure in the reactive chamber is a crucial parameter in the RFMS process and our previous results demonstrate [7] that different phases such as $LiNbO_3$, $LiNb_3O_8$ occurred in the films formed in Ar environment when partial gas pressure was equal to $P = 5.0 \times 10^{-1}$ Pa. Moreover, these polycrystalline films usually contained random-oriented grains so we decided to decrease the partial gas pressure in the reactive chamber up to 1.5×10^{-1} Pa. Films were obtained by the RFMS of monocrystalline $LiNbO_3$ target and the sputtering conditions for (001)Si-$LiNbO_3$ heterostructures are presented in Table 1.

During the RFMS process, the substrates were located over the target erosion zone (conditions for the bombardment of the substrate by high-frequency plasma ion discharge). Plates of monocrystalline silicon of (001) orientation, n-type of conductivity with resistivity of 4.5 Ohm·cm were used as substrates. For film synthesis process, the substrates were heated up to a temperature of not less than 550°C.

The study of the structure was conducted by X-ray diffraction method using Cu K_α radiation (ARL X'TRA Thermo Techno). A powder diffractometer scanned over the 2θ range from 20° to 60° with a continuous scan mode, 2 mm divergence slit, 4 mm and 0.5 mm scattering slits, and a 0.2 mm receiving slit using a line focus mirror primary optics with a Cu Kα source operated at 40 kV and 35 mA. Electrical properties of the fabricated heterostructures were studied by the methodologies based on obtaining I–V characteristics and high-frequency ($f = 10^5$ Hz) C–V characteristics in the temperature range of T = 77/290 K. The ferroelectric properties were studied by recording the hysteresis loops by the Sawyer–Tower method. The top contacts for the electrical measurements having area $S = 1 \times 10^{-6}$ m^2 were formed by thermal evaporation and condensation of Al in vacuum. The bottom electrode was created using In/Ga eutectic alloy on the Si(001) substrate providing formation of the Ohmic contacts.

Table 1. Sputtering conditions related to the studied heterostructures

Heterostructure number	Thickness of $LiNbO_3$ film, μm	Magnetron power, W	Reactive gas environment	Gas pressure, Pa	Distance between the target and bottom layer, cm
LN133	1	100	Ar	5.0×10^{-1}	5
LN134	0.37	100	Ar	1.5×10^{-1}	5
LN135	0.60	100	Ar(60%)+O_2(40%)	1.5×10^{-1}	5

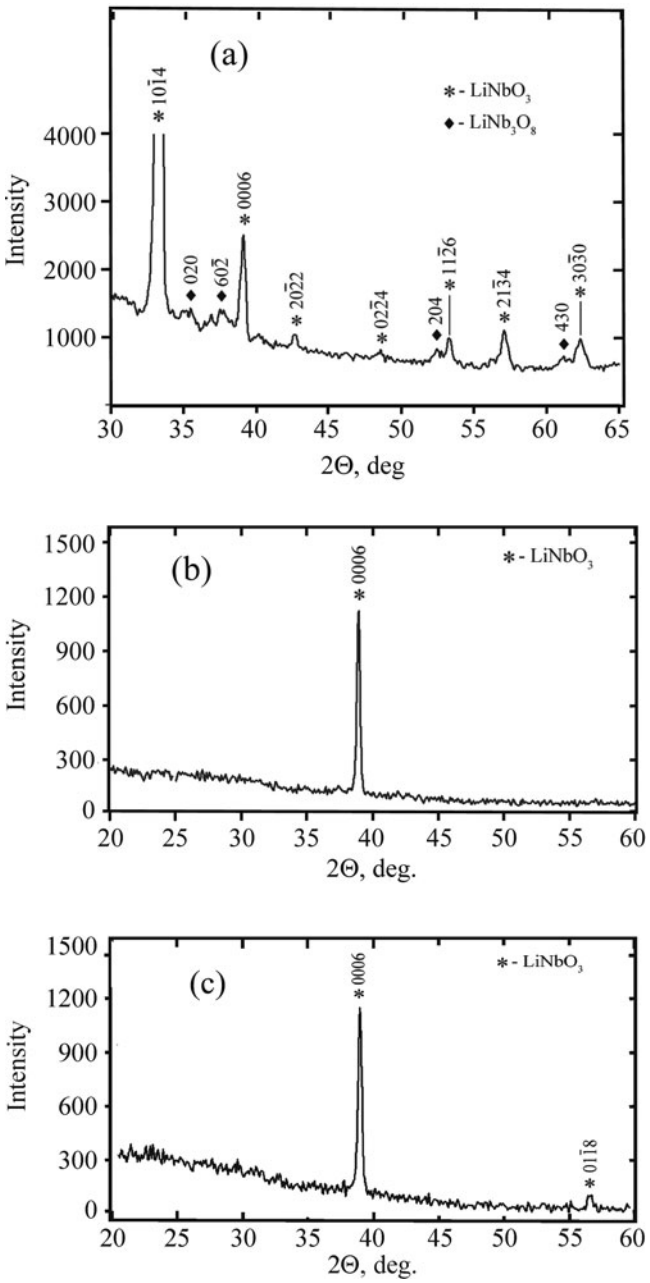

Figure 1. X-ray diffraction patterns of the films formed at different sputtering conditions (see Table 1): (a) sample LN133, (b) LN134, (c) LN135.

3. Results and Discussion

The X-ray diffraction patterns (Fig. 1(a)) demonstrated that polycrystalline films having two-phase composition ($LiNbO_3$, $LiNb_3O_8$) are formed on Si(001) substrates during the RFMS process in Ar environment for Ar pressure $P = 5.0 \times 10^{-1}$ Pa (sample LN133).

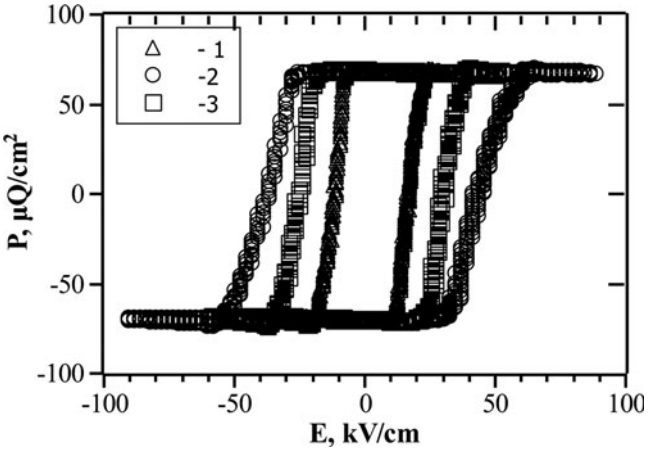

Figure 2. P–E loops of the (001)Si-$LiNbO_3$ heterostructures. 1–LN133, 2–LN134, 3–LN135.

When reactive gas pressure declines up to $P = 1.5 \times 10^{-1}$ Pa, single-phase <0001>textured polycrystalline $LiNbO_3$ films are formed on Si(001) substrates during the RFMS process (Fig. 1(b) and 1(c)), and the film's texture is the result of the ion-assisted process rather than the presence of O atoms in the reactive chamber. According to the results of the calculation by the Selyakov-Sherer method, an average grain size is equal to about 40 nm and it is close to our previous results obtained for $LiNbO_3$ films formed only in Ar environment [7, 27].

Figure 2 shows ferroelectric loops of the studied heterostructures. It can be clearly seen that remnant polarization equal to $P_r = 69\mu Q/cm^2$ does not depend on the sputtering conditions and it is close to $P_r = 71\ \mu Q/cm^2$ for bulk $LiNbO_3$. By contrast, coercive field E_c is affected by the sputtering conditions greatly, so the highest value of E_c corresponds to the sample LN134 and the lowest one to the sample LN133.

Some investigators suggested [21, 28] that the presence of defects as well as the space charge effects influence P–E loops significantly. In particular, the coercive field can be written as:

$$E_c = E_c^{/} - E_{cs} + E_{defect} \tag{12}$$

Here $E_c^{/}$ is the coercive field for the domain motion, E_{sc} is the space charge field, and E_{defect} is the dipolar effect field related to the presence of defects in the ferroelectric film. Space charge effects and defect concentration in the studied heterostructures were investigated using C–V and I–V analyses.

Figure 3 shows C–V characteristics of the studied heterostructures. We can see that C–V curves for samples LN133 and LN134 are similar to ones for MOS structure and they are shifted to the left along the voltage axis due to the presence of the positive charge in $LiNbO_3$ film. Based on the methods of C-V analysis, we derived the following value for the positive effective fixed charge: $Q_{ef} = 2{\cdot}10^{-7}$ Q/cm^2 and $Q_{ef} = 8{\cdot}10^{-7}$ Q/cm^2 for LN133 and LN134, respectively. It is important to emphasize that the sign of this charge did not depend on substrate type and was the same for $LiNbO_3$ films grown on both p-type and n-type silicon substrates [7, 12].

Regarding the sample LN135, this shift is much less than in LN134, and this fact suggests that presence of O_2 in the reactive chamber reduces positive fixed charge. Several authors revealed that oxygen vacancies formed at the Si-SiO_2 interface [29] as well as in

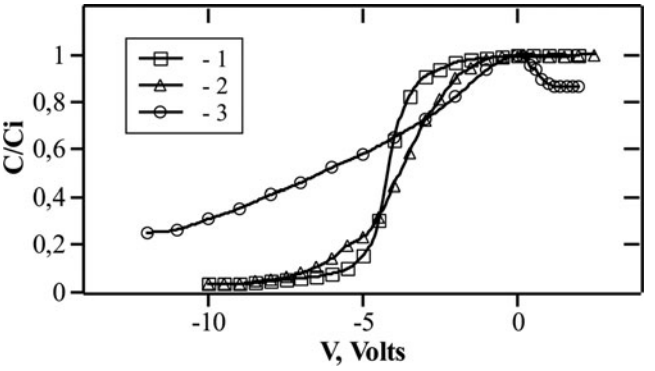

Figure 3. Normalized C–V characteristics for the (001)Si-$LiNbO_3$ heterostructures at T = 295 K. 1–LN133, 2–LN134, 3–LN135.

the bulk $LiNbO_3$ film [17] play a crucial role in formation of the positive oxide charge. Apparently, in our case introduction of oxygen atoms in the reactive ambient reduces the formation of oxygen vacancies. Moreover, C–V characteristics of LN135 sample is decreased by voltage for either polarity, and such type of dependence can exist if two depletion layers occur on both sides of the heterojunction. Such type of C–V characteristics was detailed described in the framework of two back-to-back Schottky diodes model [18]. In fact, applying voltage to the circuit of two Schottky diodes we can conclude that for either polarity of voltage the decrease of the capacitance of the reverse diode is dominant in the junction capacitance. Consequently, two branches of C–V curve accord the depletion regions in Si and $LiNbO_3$ correspondingly and a sharp maximum appears when one capacitance becomes dominant in comparison to other one. Donor concentration profile in silicon can be derived using a standard method of plotting the graph $(S/C)^2$ vs. V [30] (Fig. 4) and taking into account that it is not a straight line, we revealed that concentration profile was not homogeneous for all samples (Fig. 5).

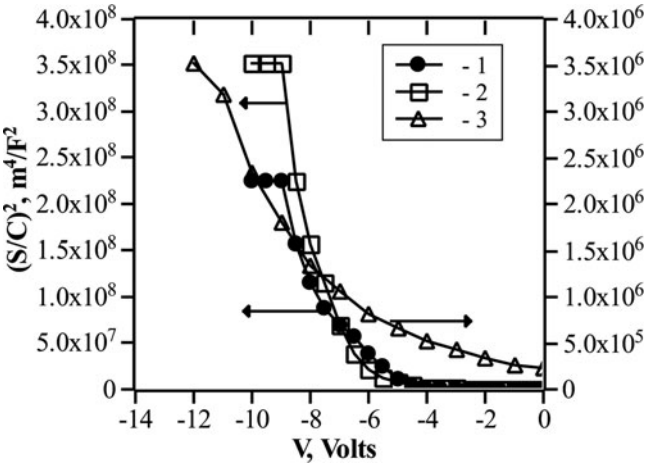

Figure 4. Plot of $(S/C)^2$ versus V for the (001)Si-$LiNbO_3$ heterostructures at T = 295 K. 1–LN133, 2–LN134, 3–LN135.

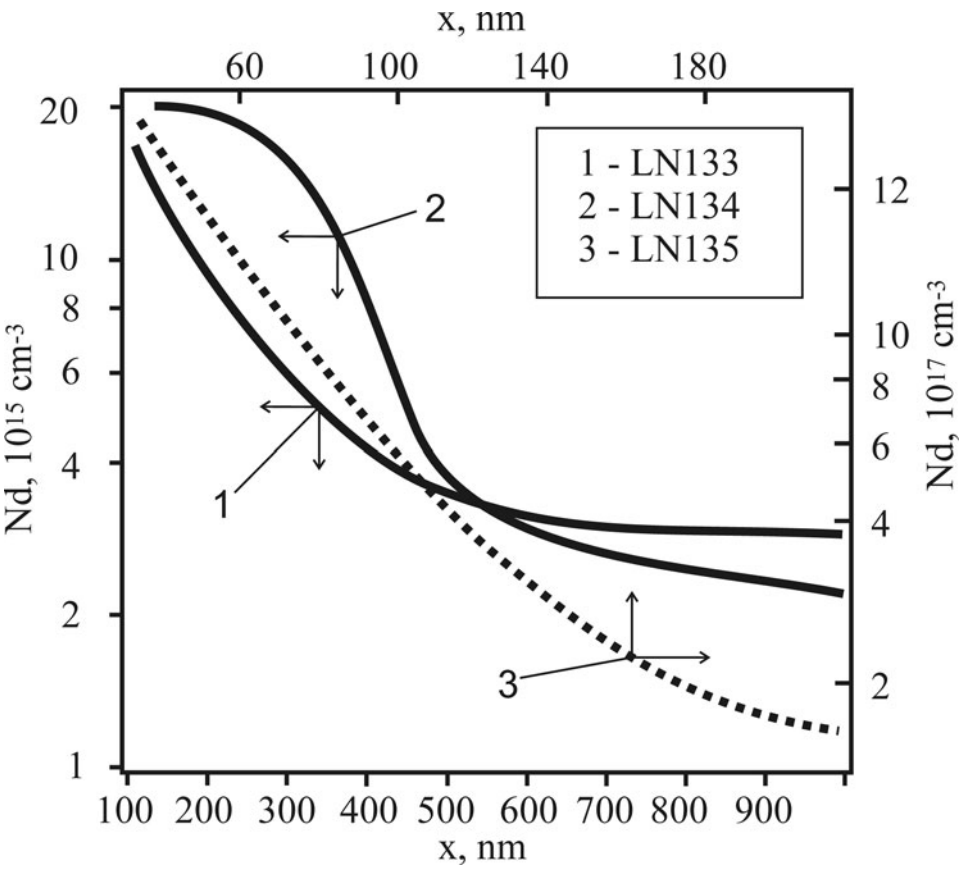

Figure 5. Donor concentration profile in silicon substrate for the studied heterostructures.

Obviously, donor concentration in silicon for heterostructures Si-$LiNbO_3$ grown in Ar+O_2 gas mixture (sample LN135) is considerably higher than in the heterostructures formed only in Ar environment (samples LN134 and LN133), and it can be explained based on the fact that fast diffusing gas-like oxygen generates thermal donors in silicon [31]. This process is very sensitive to temperature conditions because of strong dependence of oxygen diffusivity on substrate temperature and partial pressure of O_2 in the reactive chamber is a driving force of donor formation in silicon substrate. On the other hand, it was demonstrated [15] that the presence of O_2 atmosphere in the chamber influences the reactive plasma greatly in terms of increasing the concentration of the Li atoms in plasma. As a result, Li atoms being a shallow, fast-diffusing ($D = 2{\cdot}10^{-11}$ cm^2/s) donor in Si [32], penetrate into substrate not forming a homogeneous distribution of impurity. Similarly, using the graph $(S/C)^2$-V for the bias modulated the depletion region in the $LiNbO_3$ layer ("+" on $LiNbO_3$) (see Fig. 6) we obtained the donor concentration in the $LiNbO_3$ film related to the sample LN135: $N_d = 7{\cdot}10^{17}$ cm^{-3}.

I–V characteristics of the studied heterostructures (Fig. 7) demonstrate two main areas: region of the low electric field (Region I) and the region of the high electric field (Region II). Many authors described such type of I–V curve in the framework of the series of two back-to-back Schottky diodes by the formula (8) where J_s is the saturation current and V_o is

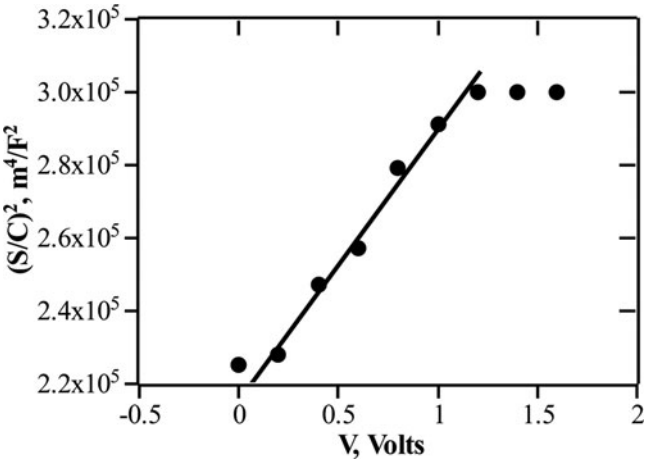

Figure 6. Plot of $(S/C)^2$ versus V related to the depletion region in $LiNbO_3$ at T = 295 K for sample LN135.

a parameter dependent on the conduction mechanism through the barrier. It can be derived from the slope of the graph ln(J) vs.V. In order to investigate the particular conduction mechanism it has been proposed to plot the graph V_o vs. kT/q [33] and for the studied heterostructures these graphs are shown in Fig. 8.

According to the classification done in [33], if the diode obeys ideal Schottky theory Vo data will lie on the straight line with unity slope and $V_o = kT/q$, but in contrast, if conduction mechanism is different from the one predicted by the ideal Shottky theory, parameter Vo is defined as follows:

$$V_o = \frac{nkT}{q} \tag{13}$$

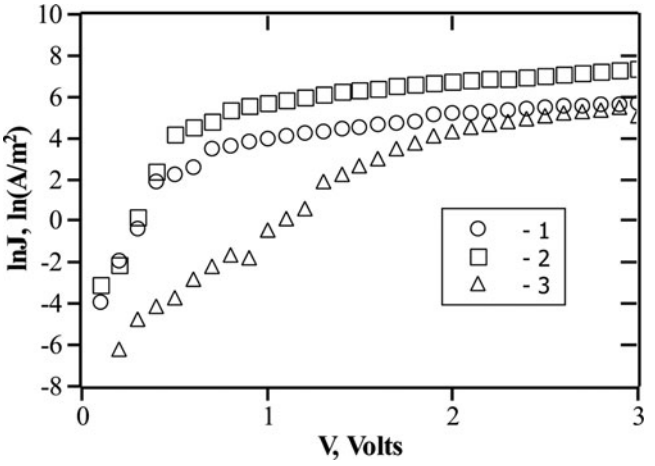

Figure 7. Typical I–V characteristics of the (001)Si-$LiNbO_3$ heterostructures at T = 295 K. 1–LN133, 2–LN134, 3–LN135.

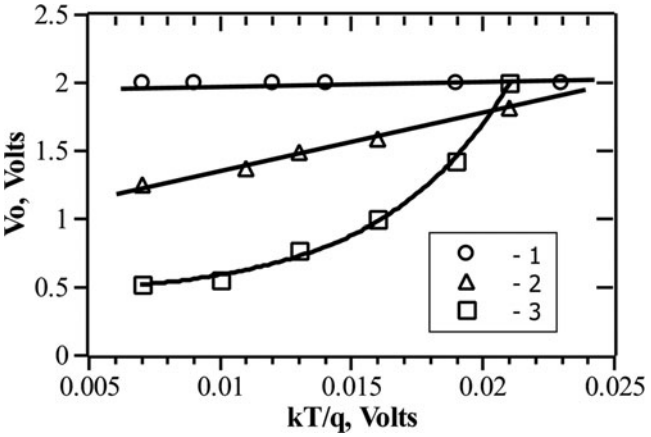

Figure 8. Plot of V_o versus kT/q for the studied heterostructures at the high electric field area (E > 3 kV/cm). 1–LN133, 2–LN134, 3–LN135.

Here n > 1 is the ideality factor (which is close to unity for the ideal Schottky theory) it depends on the conduction mechanism. For example, if Richarson-Schottky emission takes place (see formula (3)) V_o data will lie on a straight line like curve 1 in Fig. 8 with the slope equalling n:

$$n = \frac{1}{1 - \frac{\beta\sqrt{E}}{q\varphi_b}} \tag{14}$$

If thermal-assisted tunneling is a main charge transport mechanism (see (9)), V_o data will lie on a curve like the one labeled as 2 in Fig. 8. When field emission dominates V_o is independent of temperature and it will be a straight horizontal line like the one labeled as 3 in Fig. 8 and in this case $V_o = V_{oo}$ (see (10)).

Using the classification described above, it can be clearly seen from Fig. 8 that Richardson-Schottky emission is the main conduction mechanism for the sample LN 134 and graph V_o vs. kT/q is a straight line with a slope n = 40. We obtained parameter β through the graph $\ln(J/(ET^{2/3})$ vs. 1/T (not shown) as has been done in [19], and taking into account that $\varepsilon = 28$ [7] we calculated the value of the barrier height $\phi_b = 0.012$eV following the expressions (13) for the average electric field $E = 4{\cdot}10^6$ V/m. Too low value of the apparent barrier height ϕ_{app} can be explained by the fact that ferroelectric polarization P can reduce the true barrier height ϕ_b as has been mentioned earlier (see (4)). Using expressions (4) and (5) under conditions $P = 69\ \mu$C/cm^2, we obtained the recalculated value of the true barrier height $\phi_b = 0.4$ eV and effective impurity concentration $N_{ef} = 1{\cdot}10^{13}$ cm^{-3}.

As regards the sample LN135, thermal-assisted tunneling is the main mechanism of forced charge transport in this case at room temperature (although, in general, it depends on the combination temperature-electric field: see [34]). Extrapolating the value V_o when $T \to 0$ (see Fig. 8), we obtained the value V_{oo} and then concentration of ionized donors N_d via expression (10): $N_d = 4.0{\cdot}10^{18}$ cm^{-3}. Also, examination of Eq. (9) reveals that in the case of the thermal-assisted tunneling process a plot of the logarithm of J_sV_o/T vs. $1/V_o$ should be a straight line of slope ϕ_b. Such plot for sample LN135 is shown in Fig. 9 and leads to the barrier height $\phi_b = 1.25$eV.

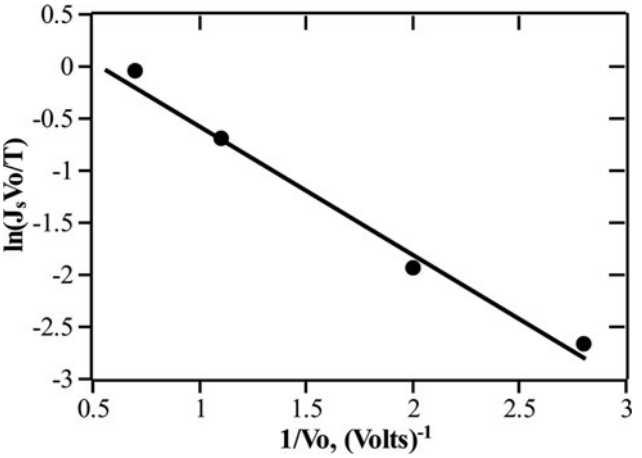

Figure 9. Plot $\ln(J_s V_o/T)$ versus $1/V_o$ for sample LN135.

As has been mentioned above, field emission affects conductivity in sample LN133 and such type of charge transport called nonactivation hopping conduction was revealed in our work [12]. In this case I–V characteristics obey the following expression:

$$J = Js \exp\left(-\left(\frac{Eo}{E}\right)^{1/4}\right) \tag{15}$$

and it should be a straight line in $ln(J)$-$E^{-1/4}$ coordinates (see Fig. 10). In (15) E is electric field and E_o is expressed by the following formula [35]:

$$Eo = \frac{\lambda}{D(E)\, a_p^4 q} \tag{16}$$

Here a_p is a polaron radius equalling $a_p \approx 3a$ [36], ($a = 5.1$Å is a lattice constant for $LiNbO_3$), *D(E)* is energy density of localized states near Fermi level, $\lambda = 1.6$ is a

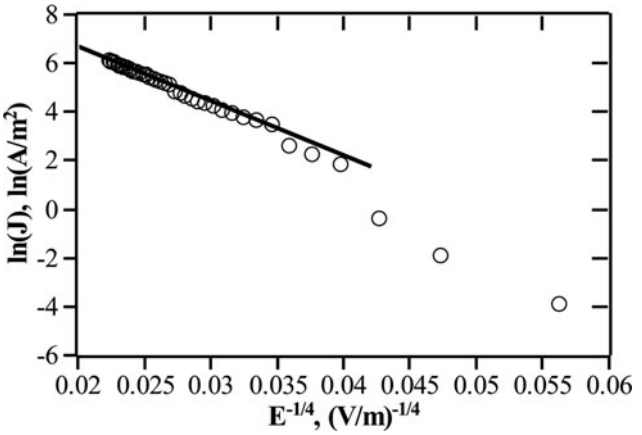

Figure 10. I–V characteristic of sample LN133 in coordinates $\ln(J)$–$E^{-1/4}$.

Table 2. Electrical properties of the $LiNbO_3$ films related to the studied Si-$LiNbO_3$ heterostructures

Heterostructure number	Donor concentration, N_d, cm^{-3}	Trap concentration, N_t, cm^{-3}	Barrier height, ϕ_b, eV	Effective oxide charge, Q_{ef}, Q/cm^2	Remnant polarization, P_r, $\mu Q/cm^2$	Coercive field, E_c, kV/cm
LN133	—	$6{\cdot}10^{17}$	—	$2{\cdot}10^{-7}$	69.0	14.0
LN134	$9{\cdot}10^{12}$	—	0.40	$8{\cdot}10^{-7}$	69.0	39.4
LN135	$7{\cdot}10^{17}$	—	1.25	$5{\cdot}10^{-8}$	69.0	27.4

dimensionless constant [37]. Also, hopping distance and effective defect concentration can be calculated using the following expressions [12]:

$$R = \frac{1}{(q \cdot D(E) \cdot E)^{1/4}} \tag{17}$$

$$N_t = \frac{2}{3\pi R^3} \tag{18}$$

Getting E_o from a slope of the graph ln(J) vs. $E^{-1/4}$ (see Fig. 10) we obtained the following results: R = 9.3 Å, $N_t = 6{\cdot}10^{17}$ cm^{-3}. To sum up, Table 2 presents the main results of C–V and I–V analysis of the studied heterostructures.

At the first sight, the sample LN 133 is the most desirable candidate among others for memory application due to the lowest coercive field and the same remnant polarization. However, as has been mentioned earlier, the lower lithium niobate phase ($LiNb_3O_8$) as well as $LiNbO_3$ one are formed at the corresponding sputtering conditions and this can be a disadvantage for many applications. It has been demonstrated [10] that Li/Nb ratio in the lithium niobate is very sensitive to gas pressure and composition. As a result, formation of the oxygen vacancies and antisite defects (Nb at Li vacancies) Nb_{Li} can be the source of positive charge and trap formation making hopping conductivity the main charge transport mechanism.

At the low Ar pressure (sample 134) the $LiNbO_3$ films become c-axes-oriented and single phase. However, as it has been pointed in [13], lithium (Li) is suspected to be highly volatile with respect to niobium (Nb) at higher sputtering pressure and may lead to the presence of large concentration of point-defects related to Li vacancies (V_{Li}). The presence of Nb antisites defect at V_{Li} may elongate the unit cell along c-axis growth direction and the deposited $LiNbO_3$ thin films are in the state of compressive stress at higher sputtering pressure. As a result, density of positive oxide charge in $LiNbO_3$ film rose significantly and coercive field increased almost three times.

When oxygen atoms are introduced in the reactive chamber, plasma composition is changed radically due to the fact that concentration of Li atoms considerably higher in $Ar+O_2$ plasma than in Ar environment [15]. Consequently, concentration of the Nb_{Li} defects as well as oxygen vacancies declined greatly which leads to decrease in coercive field and allows obtaining the lowest density of positive oxide charge.

4. Conclusions

We studied electrical properties of the Si-$LiNbO_3$ heterostructures formed by RFMS method at different sputtering conditions. Our results suggest that polycrystalline $LiNbO_3$ films

with random-oriented grains containing undesirable phase $LiNb_3O_8$ are formed in Ar environment ($P = 5.0 \times 10^{-1}$ Pa). The grown films demonstrated the lowest coercive field and the hopping non-activated conductivity originated from the presence of traps in the band gap of $LiNbO_3$ layer. Decreasing Ar pressure up to 1.5×10^{-1} Pa leads to form c-axis-oriented single-phase $LiNbO_3$ films with the highest density of positive oxide charge and coercive field. Charge transport is influenced by barrier properties at the Si-$LiNbO_3$ heterojunction, in particular, by Richardson-Shottky emission. Nonhomogeneous donor distribution is formed in Si due to diffusion of Li and O atoms into silicon and the presence of O atoms in the reactive chamber leads to increase in donor concentration in substrate by two orders of magnitude to compare with pure Ar environment. As a result, not fully depleted region is formed in $LiNbO_3$ layer and barrier properties of the Si-$LiNbO_3$ heterojunction depend on the sputtering conditions to a great extent.

Oxygen as part of the reactive gas environment has a positive impact on electric properties of the Si-$LiNbO_3$ heterostructures in terms of reduction of defects formation (as well as positive charge) in the $LiNbO_3$ films and decrease in coercive field. Nevertheless, despite the promising combination of electric properties, quite high conductivity of the sample LN135 poses a challenge to find the most optimal sputtering conditions to create the Si-$LiNbO_3$ heterostructures for memory applications.

References

[1] Nashimoto, K., Cima, M. J., McIntyre, P. C., & Rhine, W. E. (1995). *J. Mater. Res.*, *10*, 2564.
[2] Ogale, S. B., Dikshit, R. N., & Kanetkar, S. M. (1992). *J. Appl. Phys.*, *71*, 5718.
[3] Kondo, S., Miyazawa, Fusimi, S., & Sugii, K. (1975). *Appl. Phys. Lett.*, *26*, 489.
[4] Curtis, B. J., & Brunner, H. R. (1975). *Mater. Res. Bull.*, *10*, 515.
[5] Lee, T.-H., Hwang, F.-T., Lee, C.-T., & Lee, H.-Y. (2007). *Mater. Sci. Eng.*, *136*, 92.
[6] Nishida Takashi, Shimizu Masaru, Horiuchi Toshihisa, Shiosaki Tadashi, & Matsushige Kazumi. (1995). *Jpn. J. Appl. Phys.*, *34*, 5113.
[7] Iyevlev, V., Kostyuchenko, A., Sumets, M., & Vakhtel, V. (2011). *J. Mater. Sci.: Mater. Electron.*, *22*, 1258.
[8] Margueron, S., Bartasyte, A., Plausinaitiene, V., Abrutis, A., Boulet, P., Kubilius V., & Saltyte Z. (2013). In: *Oxide-based Materials and Devices IV: Proc. SPIE*, San Francisco, California, USA February, 2013, 8626, 862612.
[9] Lim, D. G., Jang, B. S., Moon, S. I., Won, C. Y., & Yi. (2001). *J. Solid-State Electron.*, *45*, 1159.
[10] Shandilya, S., Tomar, M., Sreenivas, K., & Gupta, V. (2009). *J. Phys. D: Appl. Phys.*, *42*, 095303.
[11] Ievlev, V., Sumets, M., Kostyuchenko, A., & Bezryadin, N. (2013). *J. Mater. Sci.: Mater. Electron.*, *24*, 1651.
[12] Iyevlev, V., Sumets, M., & Kostyuchenko, A. (2012). *J. Mater. Sci.: Mater. Electron.*, *23*, 913.
[13] Shandilya, S., Tomar, M., & Gupta, V. (2012). *J. Appl. Phys.*, *111*, 102803.
[14] Simo∼s, A. Z., Zaghete, M. A., Stojanovic, B. D., Gonzalez, A. H., Riccardi, C. S., Cantoni, M., & Varela, J. A. (2004). *J. Europ. Ceram. Soc.*, *24*, 1607.
[15] Gordillo-Vázqueza, F. J., & Afonso, C. N. (2002). *J. Appl. Phys.*, *92*, 7651.
[16] Cholapranee, T., & Fabiny, L. (1986). In: *Applications of Ferroelectrics: Sixth IEEE International Symposium on*, Bethlehem, PA, USA, June 1986, 585.
[17] Tsirlin, M. (2004). *J. Mater. Sci.*, *39*, 3187.
[18] Van Opdorp, C., & Kanerva, H. K. (1967). *J. Solid-State Electron.*, *10*, 401.
[19] Ievlev, V., Sumets, M., Kostyuchenko, A., Ovchinnikov, O., Vakhtel, V., & Kannykin, S. (2013). *Thin Solid Films*, *542*, 289.
[20] Simmons, J. G. (1965). *Phys. Rev. Let.*, *15*, 967.
[21] Zubko, P., Jung, D. J., & Scott, J. F. (2006). *J. Appl. Phys.*, *100*, 114112–1.

[22] Pintilie, L. (2007). *Phys. Rev. B.*, *75*, 104103.
[23] Maissel, L. (1970). *Handbook of Thin Film Technology*, McGraw-Hill: New York, USA.
[24] Padovani, F. A., & Stratton, R. (1966). *Solid-St. Electron.*, *9*, 695.
[25] Böer, K. W. (2010). *Introduction to space charge effects in semiconductors*. Springer Series in Solid-State Sciences, Vol. 160, Springer: Germany.
[26] Bartasyte, A., Plausinaitiene, V., Abrutis, A., Stanionyte, S., Margueron, S., Boulet, P., Kobata, T., Uesu, Y., & Gleize J., *et al.* (2013). *J. Phys.: Condens. Matter.*, *25*, 205901.
[27] Ievlev, V., Sumets, M., & Kostyuchenko, A. (2012). *Mater. Sci. Forum*, *700*, 53.
[28] Kim, S., & Gopalan, V. (2002). *Appl. Phys. Lett.*, *80*, 2740.
[29] Guha, S., & Narayanan, V. (2007). *Phys. Rev. Lett.*, *98*, 196101.
[30] Wikstrom, J. A., & Viswanathan, C. R. (1987). *Electron Devices, IEEE Transactions*, *34*, 2217.
[31] Gösele, U., & Tan, T. Y. (1982). *Appl. Phys. A.*, *28*, 79.
[32] Gosele, U. M. (1988). *Ann. Rev. Mater. Sci.*, *18*, 257.
[33] Saxena, A. N. (1969). *Surf. Sci.*, *13*, 151.
[34] Ievlev, V., Sumets, M., & Kostyuchenko, A. (2013). *J. Mater. Sci.*, *48*, 1562.
[35] Mycielski, (1961). *J. Phys. Rev.*, *123*, 99.
[36] Kashirina, N. I., & Lakhno, V. D. (2010). *Physics–Uspekhi*, *53*, 431.
[37] Dhar, A., Singh, N., Singh, R. K., & Singh, R. (2013). *J. Phys. and Chem. Solids*, *74*, 146.